INTERNATIONAL JOURNAL OF HYDROGEN ENERGY XXX (2018) 1–10

Available online at www.sciencedirect.com

ScienceDirect

journal homepage: www.elsevier.com/locate/he

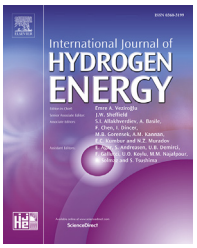

Chemical and structural optimization of $ZnCl_2$ activated carbons via high temperature CO_2 treatment for EDLC applications

Kadir Özgün Köse [a,b,*], *Berke Pişkin* [a,b,c], *Mehmet Kadri Aydınol* [a,b]

[a] *Dept. of Metallurgical and Materials Engineering, Middle East Technical University, Ankara, Turkey*
[b] *ENDAM, Center for Energy Storage Materials and Devices, Middle East Technical University, Ankara, Turkey*
[c] *Dept. of Metallurgical and Materials Engineering, Muğla Sıtkı Koçman University, Muğla, Turkey*

ARTICLE INFO

Article history:
Received 11 December 2017
Received in revised form
20 March 2018
Accepted 31 March 2018
Available online xxx

Keywords:
Biomass based materials
Activated carbon
Chemical activation
EDLC
Porosity characterization

ABSTRACT

Development of biomass based activated carbon materials for electrical double layer capacitor (EDLC) usage has gained attention as a result of requesting efficient and low cost energy storage device production. In this study, pine cone based activated carbons were produced with a combined chemical and physical activation route. $ZnCl_2$ and CO_2 were used for chemical and physical activation of the material, respectively. Activation parameters are adjusted to give different chemical and textural characteristics. FTIR and Raman spectroscopies were used for functional group identification and structural order characterization, respectively. As a result, efficient active materials for EDLC usage were obtained, with as high as 87 F/g specific capacitance in organic electrolytes.

Introduction

The demand for designing new electrochemical energy storage systems or optimizing the existing ones is increasing due to the necessity of reducing fossil fuel consumption. Chemical and structural modification of active materials are regarded as a key to overcome this problem in many studies based on energy storage systems such as Zn-air batteries and supercapacitors [1–4]. EDLC takes an important place among other energy storage devices considering its efficient energy storage mechanism and prolonged cycle life. It is characteristically a high power device, suffering from low energy density. The increasing use of EDLC mainly depends on either enhancement of its energy density, or construction of a hybrid system with a characteristically high energy device, such as fuel cell [5–8]. Therefore, optimizing the properties of EDLC is of paramount importance for both scientific and technological research.

The choice of appropriate active material in electrode is a key factor in efficient electrochemical energy storage device development. In this regard, activated carbon is one of the most widely utilized material with tunable pore size, high surface area and good electronic conductivity. Besides its dominating role in EDLC electrodes, it is a promising material for fuel cell applications due to high hydrogen adsorption capacity [9–11]. In this study, activated carbon was produced from cone of Pinus pinea, which was reported as a promising

* *Corresponding author*. Dept. of Metallurgical and Materials Engineering, Middle East Technical University, Ankara, Turkey.
E-mail address: kose@metu.edu.tr (K.Ö. Köse).

https://doi.org/10.1016/j.ijhydene.2018.03.222
0360-3199/

material for activated carbon production due to its low ash content [12]. Carbonization behavior of pine cone was studied by Haykırı-Açma [13], and 9.4 wt% moisture, 69 wt% volatile matter, 20.9 wt% fixed carbon and 0.7 wt% ash was reported. Ash in biomass is electronically inactive and blocks the pore entrances during activation [14]. Therefore, low ash content Pinus pinea cone was chosen for biomass precursor. Despite its suitable characteristics, there are few reports based on pine cone based activated carbon used in EDLC applications [15–17]. In the article published by Karthikeyan et al. [15], pine cone derived activated carbons were used for construction of EDLC's with 1 M $LiPF_6$ dissolved in EC/DEC electrolyte, and as high as 61 Wh/kg energy density was achieved. However, there is no study on its usage with quaternary ammonium salts in acetonitrile, to the best of our knowledge.

In classical understanding of the double layer, surface area must be increased in order to achieve high energy density according to Helmholtz model, which states the relationship between capacitance (C), vacuum permittivity (ε_0), relative permittivity of the electrolyte (ε_r), surface area of the electrode (S) and effective thickness of the double layer (d), by Equation (1):

$$C = \varepsilon_0 \varepsilon_r \frac{S}{d} \quad (1)$$

Furthermore, electronic conductivity of the electrode material must be high to decrease equivalent series resistance (ESR), which is related to maximum power (P_{max}) by Equation (2):

$$P_{max} = \frac{V^2}{4ESR} \quad (2)$$

Earlier studies on EDLC performance of activated carbons mainly focused on the specific surface area. It was emphasized that the more specific surface area the activated carbon has, the more specific capacitance can be achieved, within the context of Helmholtz model. However, there appears to be a plateau when specific surface area vs. specific capacitance graphs are plotted for activated carbons having surface areas greater than 1200 m^2/g [18]. Therefore, it is necessary to adjust porosity characteristics of activated carbons according to present ions in the electrolyte. This adjustment can be made by tuning activation steps.

Among all the activating agents, $ZnCl_2$ and KOH are the most widely used ones to produce activated carbons for EDLC. In a recent study, $ZnCl_2$ and KOH were used for activated carbon production from wheat straw. It was stated that unlike KOH, $ZnCl_2$ evenly distributed through precursor, preventing hyper-activation [19]. Therefore, $ZnCl_2$ was chosen as activating agent to have better control on porosity creation. There are numerous studies based on $ZnCl_2$ activation of biomass in EDLC applications including cotton [20], tea-leaves [21], rice husk [22], waste coffee ground [23] and peanut shell [24]. Rufford et al. [23] reported as high as 1021 m^2/g BET surface area was achieved in coffee ground based activated carbons, and they yielded nearly 100 F/g specific capacitance at fast charge-discharge rates in $TEABF_4$/ACN electrolyte. In another study, He et al. [24] achieved 1634 m^2/g BET surface area by microwave assisted $ZnCl_2$ activation method and the resulting activated carbons bring about as high as 99 F/g specific capacitance in $TEABF_4$/PC electrolyte.

Impregnation ratio was reported as the most important parameter in $ZnCl_2$ activation [25]. CO_2 treatment on $ZnCl_2$ activated carbons was also studied [26,27]. As a result of porosity shrinkage, an initial decrease in surface area was observed and surface area gradually increased as high burn off degrees were achieved. Together with the effect of impregnation ratio on porosity, CO_2 treatment is a suitable method to obtain activated carbon with various textural properties. Furthermore, different activation mechanisms bring about different structural order and surface chemistry in activated carbons, particularly influential on electrical conductivity. Hence, it is aimed to produce pine cone based activated carbons with various chemical and structural properties, and analyze their electrochemical behavior. A low temperature $ZnCl_2$ activation followed by high temperature CO_2 treatment was chosen to achieve this goal.

Materials and methods

Pine cone (pinus pinea) was held in ethyl acetate for 48 h to remove the stuck resin stuck on it. After removal of the resin layer, pine cone was dried in open atmosphere for several days. Dried cones were crushed and ball milled at 200 rpm for 15 min, and sieved to 50 mesh. Then, pine cone powder was mixed with $ZnCl_2$ aqueous solution with precursor to activating agent mass ratio of 1:1 and 1:4 (to obtain 1 and 4 impregnation ratio, respectively) and mixed with magnetic stirrer at 110 °C. The impregnated samples were dried overnight at the same temperature. The activation step was carried out in a horizontal tube furnace, under N_2 gas at a flow rate of 0.2 lt/min. The activation temperature and time were 500 °C and 2 h, respectively. After the activation step completed, samples were washed first with 1-M HCl and then hot distilled water, until pH value of 6.5–7 was reached. The samples were designated as IR1 and IR4, indicating impregnation ratio. Further activation with CO_2 was conducted at a flow rate of 0.5 lt/min CO_2 gas, at 800 and 900 °C. Activation times were 12 and 36 h for 800 °C and 5 h for 900 °C. CO_2 treated samples were designated as IR1-c12, IR1-c36, IR4-c12, IR4-c36 for 800 °C, indicating activation time, and IR1-c900 and IR4-c900 for 900 °C, remarking activation temperature.

N_2 adsorption was applied to AC's in Autosorb-6 at 77 K. Before the measurement, samples were kept in vacuum at 200 °C for 3 h, in order to remove the gases adsorbed onto them (degassing). Surface area and pore size distribution was calculated in Quantachrome Autosorb software. Pore size distribution calculation is conducted using QSDFT equilibrium model for N_2 at 77 K on carbon for slit pore geometry, given in the software. Average pore size was calculated using weighted average of cumulative surface area. Raman spectroscopy was applied using Renishaw inVia Raman spectrometer with a 532 nm wavelength laser. Deconvolution of the peaks is conducted using 2 Lorentzian peaks for D and G bands. FTIR spectroscopy was applied using Perkin Elmer Frontier spectrometer in attenuated total reflectance (ATR) mode. Background was subtracted before spectrum was obtained. Analyses were performed in directly to samples, without any addition. An apparatus was designed for direct electrical conductivity measurement from powders. Two brass plugs, in

Please cite this article in press as: Köse KÖ, et al., Chemical and structural optimization of $ZnCl_2$ activated carbons via high temperature CO_2 treatment for EDLC applications, International Journal of Hydrogen Energy (2018), https://doi.org/10.1016/j.ijhydene.2018.03.222

between the powder to be measured, were fixed with clips, and the region where powders reside was isolated with a PEEK cylinder. After this apparatus was assembled, electrical conductivities of samples were measured in Modulab MTS Solartron Analytical for the module suitable for highly conductive materials. Conductivity was measured in DC current at a constant voltage of 5 mV for 10 min.

Produced activated carbons were ball milled for 15 min to achieve uniform particle size distribution. Samples were mixed with conductive additive (carbon black) and PSBR 100 binder so as to have 80:10:10 weight percent ratio, respectively. The obtained slurry was tape cast on Ni foil. After completely dried, electrodes were cut into 18 mm stamps. Typical active material loading was about 8 ± 1 mg/cm^2.

Cells were constructed in a glove box, having H_2O and O_2 content of less than 0.1 ppm. Glass fiber separators were used in cell construction. The electrolytes used in this study were 1-M $TEABF_4$ and 0.3-M $TBAPF_6$ dissolved in acetonitrile. Two electrode symmetric cells were used in this study. Cyclic voltammetry was carried out with 10, 30 and 50 mV/s scan rates between 0 and 2.7 V using a Biologic VMP 300 potentiostat. Specific capacitances were calculated according to Equation (3):

$$C_{cv}(F/g) = \frac{\int I(V)dV}{2mVv} \quad (3)$$

where I is current in A, V is voltage in V, v is scan rate in V/s, m is total active mass in g.

Results & discussion

Characterization of activated carbons

Determination method of surface area and pore size distribution of activated carbon has been a subject of controversy. Although BET model is widely used for surface area calculation, it overestimates surface area, especially when used in the relative pressure range of 0.05–0.3 for microporous solids. Kaneko et al. [28] reported that restriction of the relative pressure range to lower relative pressures gives rise to more realistic results of BET surface area when applied to microporous carbons. Therefore, relative pressure range of 0.01–0.1 was used in this study for BET surface area.

Among various methods to evaluate pore size distribution of activated carbons having both micro and mesoporosity, DFT methods are considered to be the most reliable. NLDFT and QSDFT methods were both used in various researches; however, NLDFT gave a false gap around 1 nm [29]. Therefore, QSDFT method was used for analyzing pore size distribution in this study.

Fig. 1 represents adsorption isotherms of produced activated carbons for N_2 at 77 K (a and b) and their pore size distributions (c and d). According to BDDT classification [30], IR1, IR1-c12, IR1-c36 and IR1-c900 have type 1 isotherm characteristic of microporous adsorbents, while IR4, IR4-c12, IR4-c36 and IR4-c900 show type 1–4 hybrid isotherm shape, indicating

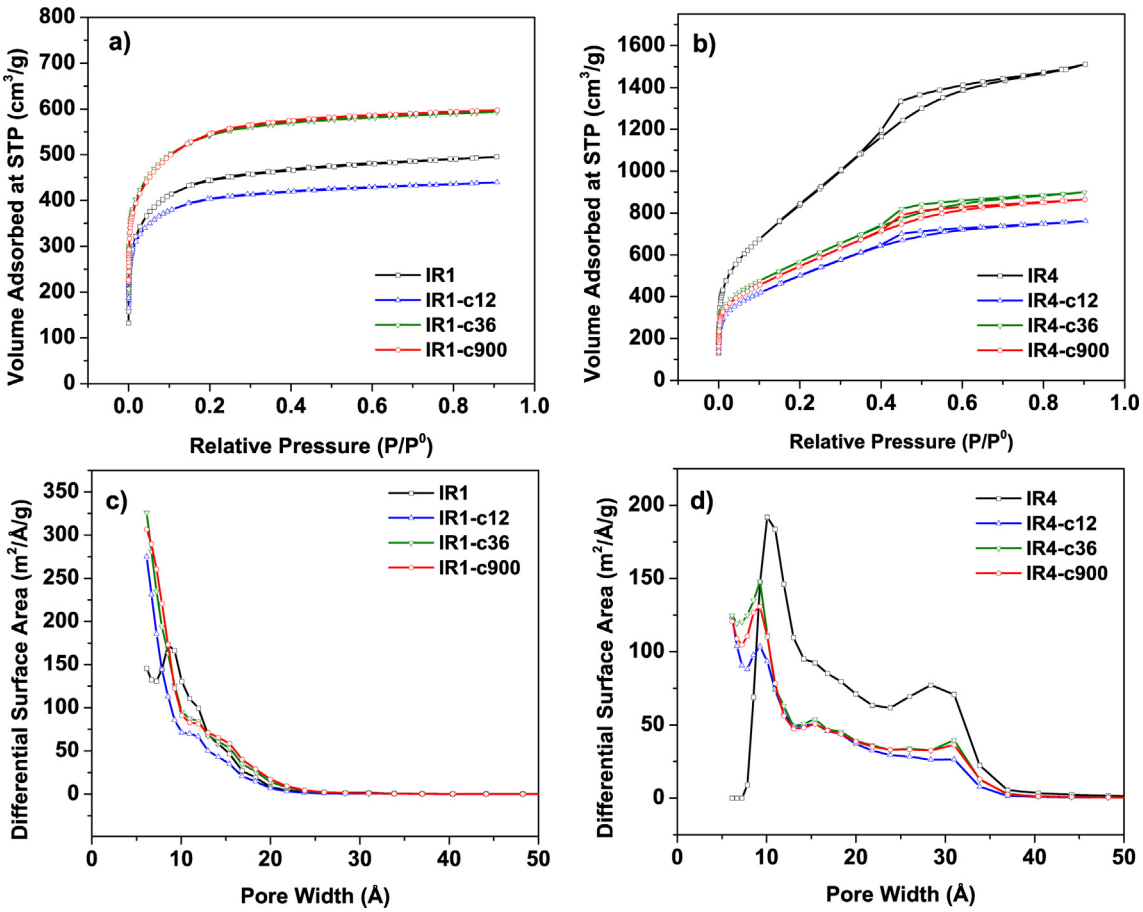

Fig. 1 – Adsorption isotherms (a and b) and pore size distributions (c and d) of activated carbons.

Please cite this article in press as: Köse KÖ, et al., Chemical and structural optimization of $ZnCl_2$ activated carbons via high temperature CO_2 treatment for EDLC applications, International Journal of Hydrogen Energy (2018), https://doi.org/10.1016/j.ijhydene.2018.03.222

Table 1 – Surface area, pore volume and burn off degree of activated carbons.

Samples	S_{BET} (m^2/g)	S_{DFT} (m^2/g)	S_{mic} (m^2/g)	S_{meso} (m^2/g)	V_{mic} (cm^3/g)	V_{meso} (cm^3/g)	Burn off %
IR1	1666	1407	1373	32	0.65	0.05	–
IR1-c12	1513	1465	1444	20	0.59	0.03	14
IR1-c36	2007	1891	1853	37	0.8	0.04	28
IR1-c900	2001	1825	1784	40	0.8	0.05	34
IR4	2771	2218	1323	870	0.9	1.22	–
IR4-c12	1692	1512	1157	347	0.61	0.47	15
IR4- c36	1919	1714	1263	442	0.66	0.63	30
IR4-c900	1839	1652	1214	430	0.64	0.59	36

mesoporosity. Consistent with previous studies [31,32], impregnation ratio has a quite pronounced effect on pore structure; 1 impregnation ratio samples are mainly microporous, while 4 impregnation ratio ones have a considerable amount of mesoporosity along with microporosity as a result of pore widening. Furthermore, CO_2 treatment affected porosity; although it did not change the type of the isotherm, textural properties greatly differed with activation time and temperature. Burn off degree reveals the extent of activation and it has a remarkable influence on surface area and pore volume creation. Both micropore and mesopore volume of IR4 decreased when CO_2 treated; greater effect was seen in the mesopores. When the burn off degree increased, development of mesoporosity was evident as seen in IR4-c36 and IR4-c900 samples. However, CO_2 treated samples could not reach the initial mesopore volume and surface area of IR4. Considering the fact that increasing microporosity and surface area of the activated carbon increases hydrogen adsorption [9], IR4 can be the most promising material for hydrogen storage. On the other hand, sample with 1 impregnation ratio developed both surface area and pore volume as a result of high burn off degree CO_2 treatment. This is evident in IR1-c36 and IR1-c900, while porosity narrowed down and pore volume decreased in the low burn off treatment in IR-c12, as seen in Table 1.

This porous structure difference with the extent of CO_2 activation can be ascribed to competition between porosity shrinkage and physical activation by CO_2. As a result of the structural reorganization, activated carbon densifies when heat treated at a temperature higher than activation temperature, therefore pore structure collapses. However, if CO_2 activation proceeds, this effect is eliminated and physical activation with CO_2 dominates the textural properties. Although BET surface area calculations were restricted to 0.01–0.1 relative pressure range, the S_{BET} values were substantially greater than values given by DFT. As a more reliable assessment, values given by DFT calculations were used in the electrochemical characterization.

Surface functional groups on activated carbon greatly alter the electrochemical response when used in electrochemical capacitors. Their most important effects are reducing the conductivity of activated carbons and creating pseudocapacitance. To analyze them, IR spectroscopy, a widely used technique for qualitative evaluation of surface functional groups of carbon materials, was applied and results are given in Fig. 2.

In the spectra, all the specimens have broad absorption bands around 1730, 1240, 1150 and 1080 cm^{-1}. Additionally, samples IR1 and IR4 have adsorption bands at nearly 1580, 875, 800 and 750 cm^{-1}. The intensities of these bands are greater on sample IR4, and after the heat treatment, intensities of all the bands greatly reduce. Moreover, 1580, 800 and 750 cm^{-1} bands completely disappear in CO_2 treated samples. The precise assignment of surface functional groups in the FTIR spectrum is not straightforward. Since carbons absorb most of the radiation, and also the FTIR assignments of different functional groups are very close to one another, complex bands of the spectra should be interpreted with caution [33]. The band around 1730 cm^{-1} is ascribed to C=O stretching vibrations of carbonyl groups, carboxylic acids and anhydrides, and lactones [34]. 1580 cm^{-1} band is associated with C=C stretching vibration in aromatic rings and quinones [35,36]. C–O stretching mode of carboxylic acids and O–H

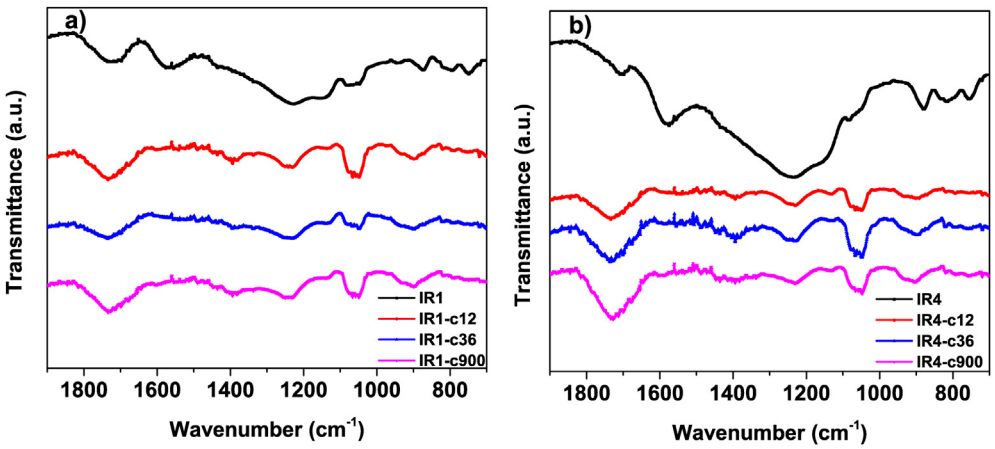

Fig. 2 – FTIR spectra of (a) 1 IR, (b) 4 IR activated carbons.

Please cite this article in press as: Köse KÖ, et al., Chemical and structural optimization of $ZnCl_2$ activated carbons via high temperature CO_2 treatment for EDLC applications, International Journal of Hydrogen Energy (2018), https://doi.org/10.1016/j.ijhydene.2018.03.222

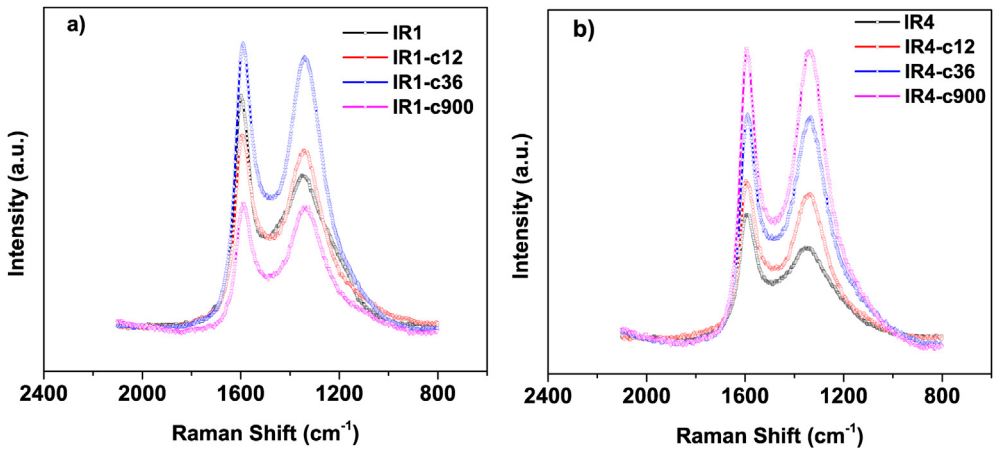

Fig. 3 – Raman spectra of (a) 1 IR, (b) 4 IR activated carbons.

bending mode are responsible for 1240 and 1150 cm^{-1} bands, respectively [37,38]. Finally, C–H out of plane vibration gives rise to 875, 800 and 750 cm^{-1} peaks [39]. The reduction in the intensity of the bands, even their disappearance, is a consequence of decreasing the surface functional group content of the activated carbons after heat treatment. However, the size of aromatic ring structure increases as the heat treatment temperature is enhanced. The disappearance of the 1580 cm^{-1} band of the CO_2 heat treated samples does not result from the lower size of the aromatic ring clusters, rather it is due to the dipole moment increase of aromatic ring vibrations with the presence of surface oxygen atoms. Consequently, amount of surface functional groups of the activated carbons effectively reduced via high temperature CO_2 heat treatment.

Decrease in the surface oxygen functional groups of the activated carbons affect electrochemical energy storage systems in a different manner. On one hand, while oxygen functionalities introduce pseudocapacitive contributions especially in aqueous electrolyte EDLC's, they also result in electrical conductivity decrease in activated carbons. On the other hand, their presence increase hydrogen uptake, as claimed in a recent study [40]. Therefore, sample IR4 is considered as a most promising candidate for hydrogen storage applications, due to not only by its high surface area, but also its high amount of surface functional groups.

Fig. 3 displays Raman spectra of activated carbons, indicating characteristics of disordered carbon materials. They constitute a broad D band and a relatively sharp G band. G band was typically interpreted as a measure of order, whereas D band was considered to reflect disorder. The origin of G band is E_{2g} vibration mode of sp^2 bonded carbon atoms. The D band is associated with A_{1g} breathing mode, which is not allowed in single crystal graphite, only possible with the presence of disorder. Therefore, Tuinstra and Koenig [41] offered I(D)/I(G) ratio as a parameter to assess the order of carbon materials, being inversely proportional to crystallite size. In a later work, Ferrari and Robertson [42] proposed a three stage model according to amorphization of carbon materials, from single crystal graphite to tetrahedral amorphous carbon with 100% sp^3 bonding. They argued the intensity of the D band is associated with the existence of six folded rings, which increases with the increase of sp^2 bonded cluster size. Therefore, I(D)/I(G) ratio increases with more ordered structure with greater sp^2 cluster area in the stage 2 of their model, from amorphous carbon to nanocrystalline graphite.

Another parameter to be considered to determine the structural order of activated carbons using Raman spectroscopy is full width at half maximum (FWHM) of the D band. Narrowing down of the D band was linked to the enhancement of the structural order, due to the reduction of contributions from the distribution of amorphous carbon structures within ordered structure [18] and bond angle disorder [43]. Table 2 represents the intensity ratios of D and G bands, and FWHM of the D band of the activated carbons. As previously reported [44], the effect of porosity on the order of the activated carbon is not pronounced; slight increase in intensity ratio and decrease in FWHM of D band is attributed to difficulty in representing these spectra with 2 peak fits and experimental errors. The stronger effect is seen on the heat treatment; I(D)/I(G) ratio increases and FWHM of D band decreases significantly as heat treatment temperature or time increases. This consequence clearly shows that CO_2 heat treated samples have much larger sp^2 domains and more ordered structure.

One of the most important parameters that determine EDLC performance of activated carbons is electrical conductivity. The structure and surface functional groups of activated carbons have a great influence on electrical conductivity, as seen in Table 3. In the model suggested by

Table 2 – I(D)/I(G) ratio and FWHM of D band, calculated by 2 Lorentzian peak fits.

Samples	I(D)/I(G)	FWHM (D) cm^{-1}
IR1	0.72	262.2
IR4	0.80	251.9
IR1-c12	0.99	219.8
IR4-c12	0.99	202.8
IR1-c36	1.04	204.4
IR4-c36	1.05	212.8
IR1-c900	1.04	195.4
IR4-c900	1.06	191.9

Please cite this article in press as: Köse KÖ, et al., Chemical and structural optimization of $ZnCl_2$ activated carbons via high temperature CO_2 treatment for EDLC applications, International Journal of Hydrogen Energy (2018), https://doi.org/10.1016/j.ijhydene.2018.03.222

Table 3 – Electrical conductivities of activated carbons.

Samples	Conductivity (S/cm)
IR1	2.1×10^{-5}
IR4	2.6×10^{-5}
IR1-c12	0.60
IR4-c12	0.34
IR1-c36	0.37
IR4-c36	0.32
IR1-c900	0.74
IR4-c900	0.60

Mrozowski [45], electronic energy band of carbons are given as a function of heat treatment temperature. The reduction of band gap, and consequently increase in conductivity is associated with delocalized electrons of π bonds, which reside in sp^2 clusters of aromatic rings. The Raman spectra of the activated carbons indicate that sp^2 cluster size increases after high temperature CO_2 treatment with aromatic ring condensation. Furthermore, surface oxygen groups decrease electronic conductivity of activated carbons, since they occupy the edges of the microcrystalline domains and blocking the electron transfer [46]. FTIR spectra of the produced activated carbons provide evidence to decrease surface oxygen groups upon CO_2 heat treatment. As a result, electronic conductivities of CO_2 treated samples increased 5 orders of magnitude, for higher sp^2 cluster size and lower surface oxygen content.

Electrochemical characterization

Cyclic voltammograms of only $ZnCl_2$ activated carbons (samples IR1 and IR4) with $TEABF_4$ in acetonitrile electrolyte are given in Fig. 4. The figure demonstrates that the samples show resistive behavior instead of typical quasi-rectangular voltammograms of carbon materials.

In a previous study [47], similar treatments with $ZnCl_2$ resulted in similar cyclic voltammetry responses. They concluded this response resulted from the porous structure of the carbons produced. In fact, this may have an effect on the resistive behavior, as sample IR4 with a pronounced mesoporosity achieved higher current densities especially in higher applied voltages. However, the 5 orders of magnitude increase in the electrical resistivity when compared with CO_2 treated carbons clarifies that the main contribution to overall resistance of EDLC comes from the resistivity of the activated carbons. Furthermore, higher amount of oxygen functional groups in sample IR4 can have a pseudocapacitive effect on electrochemical behavior, which can be the reason for high current density in high potential difference. Consequently, the specific capacitance obtained in only $ZnCl_2$ activated carbons were smaller than CO_2 treated ones. It was only 22 F/g for IR4 calculated from voltammogram at a scan rate of 10 mV/s.

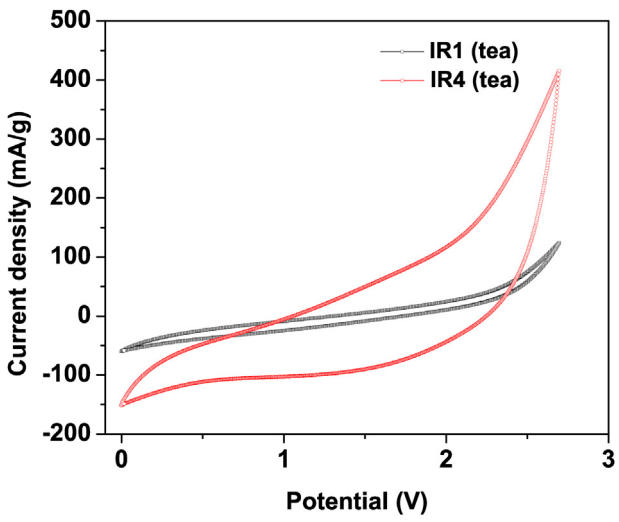

Fig. 4 – Cyclic voltammograms of samples IR1 and IR4 with TEA BF_4 electrolyte at a scan rate of 10 mV/s.

Having discussed the effect of CO_2 treatment on the physical and chemical properties of the activated carbons, its consequence on the electrochemical properties is evident on the cyclic voltammograms given in Fig. 5. The quasi rectangular shapes of the voltammograms are attributed to their electrical conductivity increase, as discussed. Further, the current density response differences upon applied voltage are strongly influenced by ion pore interactions. The impact of pore structure on the double layer performance of carbons has been a subject of controversy. In an earlier approach, ions are accepted as in their solvated state at the double layer. Therefore, carbons having pore widths greater than 1 nm is argued to be superior in EDLC's. More recently, microporous carbons with smaller average pore sizes and narrower pore size distributions are suggested to have higher specific capacitance per unit area [48]. This behavior originates from desolvation of ions in their charged state [49]. Therefore, bare ion sizes (TEA^+:0.68 nm, TBA^+:0.82 nm) are used in this study to evaluate electrochemical behavior [50]. Fig. 5 remarks that current densities reached by EDLC's using $TEABF_4$ electrolyte are superior to EDLC's with $TBAPF_6$. Considering bare ion sizes of TEA^+ and TBA^+ cations, the effective surface areas ($S_{DFT} > 0.68$ and $S_{DFT} > 0.82$) that is available for double layer formation differ substantially, being greater for TEA^+ cation. As a result, specific capacitance reached with $TEABF_4$ salt is higher, due to more open surface for TEA^+ electroadsorption. Moreover, current densities of carbons with different pore characteristics are similar in $TEABF_4$ electrolyte, while capacitive current drops as the voltage is increased in $TBAPF_6$. Pore saturation, complete coverage of the available surface before reaching the maximum voltage as a result of insufficient development of porosity, is the reason of the capacitance reduction in high voltages [51]. Comparing CV results of 4 impregnation ratio and 1 impregnation ratio samples with $TBAPF_6$ electrolytes, high effective surface area values of the former ones for TBA^+ electroadsorption prevents saturation of porosity, while the latter ones exhibit this current decrease, being more pronounced for IR1-c12.

Specific capacitances are drawn as a function of DFT specific surface areas of activated carbons in Fig. 6. There is no trend found in the specific capacitance values as specific surface area changes, consistent with previous studies [18,52]. The lack of capacitance enhancement with increasing surface area was attributed to the charge screening in the article proposed by Barbieri et al. [18]. It was argued that development of surface area diminishes pore wall thickness, thus, electric potential within the pore does not reach zero. This

Please cite this article in press as: Köse KÖ, et al., Chemical and structural optimization of $ZnCl_2$ activated carbons via high temperature CO_2 treatment for EDLC applications, International Journal of Hydrogen Energy (2018), https://doi.org/10.1016/j.ijhydene.2018.03.222

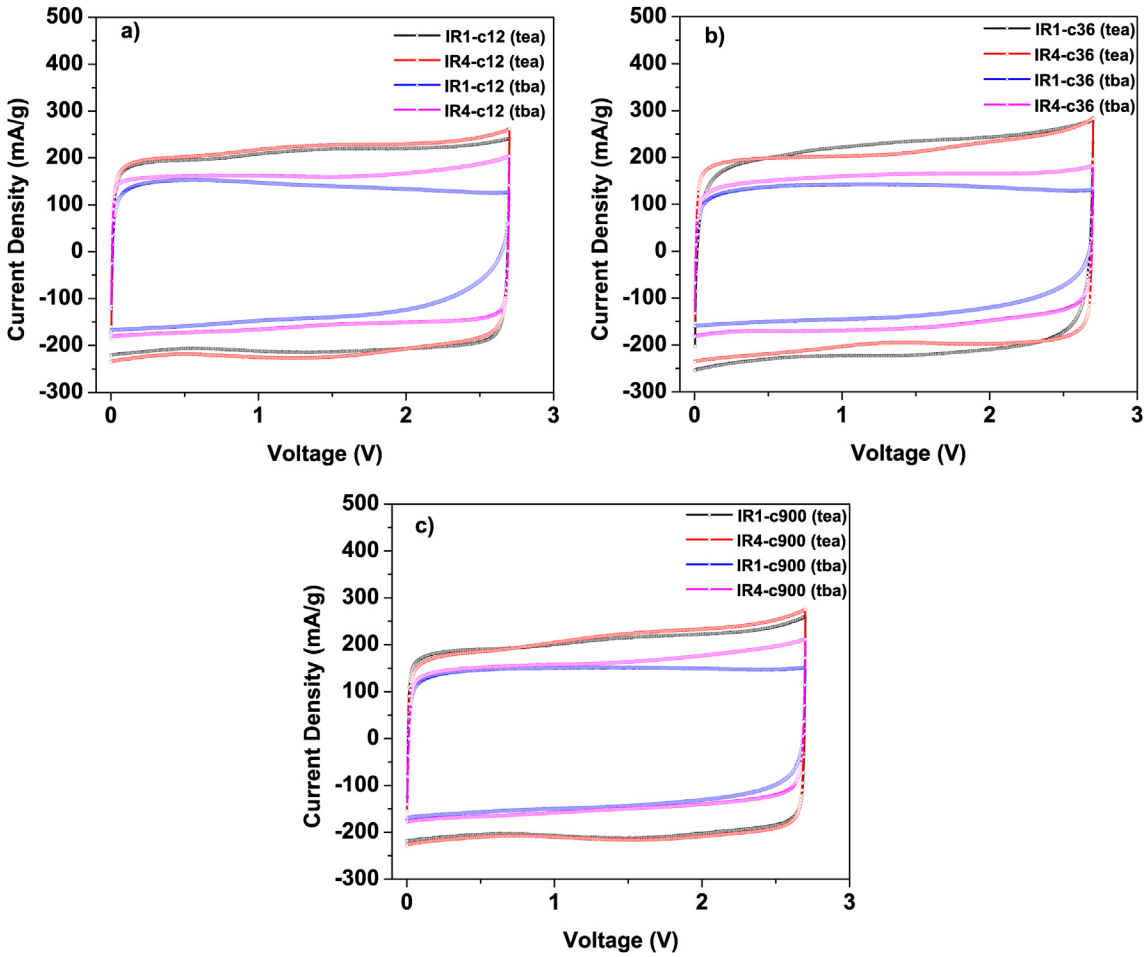

Fig. 5 – Cyclic voltammograms of CO_2 treated carbons with TEA BF_4 and TBA PF_6 electrolyte, (a) carbons treated at 800 C for 12 h, (b) carbons treated at 800 C for 36 h, (c) carbons treated at 900 C for 5 h, scanned at a rate of 10 mV/s.

situation deteriorates capacitive behavior so that specific capacitance remains constant for carbons having specific surface areas larger than 1200 m^2/g, no matter how specific surface area enhances.

The capacitive properties of the carbons were further analyzed with normalizing specific capacitance values by available surface areas as seen in Table 4. Similar trends are observed for both electrolytes: a dramatic reduction of capacitance with enhancement of the average pore size, L_0. Ineffective usage of pore volume in wide pores brings about this reduction in normalized capacitance [53]. Furthermore, although the trend is similar, EDLC's with $TEABF_4$ electrolyte have high normalized capacitance for all samples. This is linked to the bigger size of the TBA^+ cation, increasing the distance between electrode surface and ions. Specific capacitance change as a function of scan rate is given in Table 5. Specific capacitance reduction with increasing scan rate was observed for all samples. The reason of this reduction is the limitation of the ion diffusion at high rates of charge and discharge. Due to limited diffusion, some of the ions do not have enough time to reach electrode surface and form double layer, so that capacitance decreases. However, a relatively stable behavior arises in the EDLC's with $TEABF_4$ electrolyte. Diffusion is more restricted for TBA^+ ions in the $TBAPF_6$ electrolyte due to its bigger size and low concentration, therefore its capacitance reduction is more pronounced with increasing scan rates. Furthermore, porous structure affects capacitive response as a function of scan rate; greater

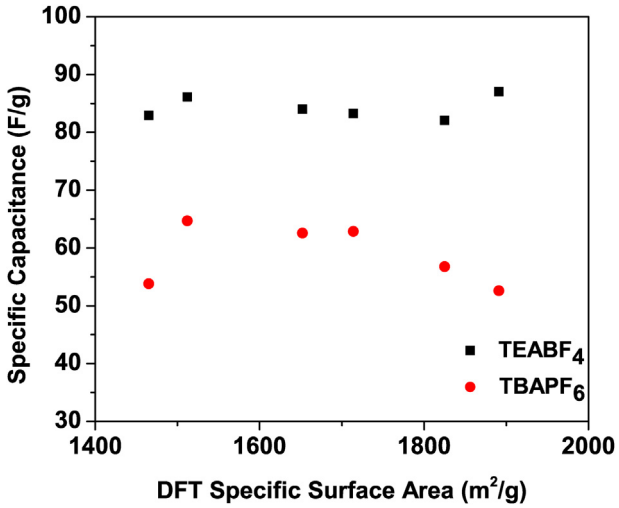

Fig. 6 – Specific capacitance vs. specific surface area of the activated carbons.

Please cite this article in press as: Köse KÖ, et al., Chemical and structural optimization of $ZnCl_2$ activated carbons via high temperature CO_2 treatment for EDLC applications, International Journal of Hydrogen Energy (2018), https://doi.org/10.1016/j.ijhydene.2018.03.222

Table 4 – Average pore sizes, available surface areas and normalized capacitances of the activated carbons.

Samples	L_0 (nm)	$C^+_{TEA}/(S_{DFT}>0.68)$ ($\mu F/cm^2$)	$C^+_{TBA}/(S_{DFT}>0.82)$ ($\mu F/cm^2$)
IR1-c12	0.89	11.4	10.4
IR1-c36	0.93	8.5	7.1
IR1-c900	0.96	7.6	7.3
IR4-c12	1.49	7.4	6.3
IR4-c36	1.55	6.0	5.2
IR4-c900	1.55	6.3	5.4

Table 5 – Specific capacitances evaluated in cyclic voltammetry as a function of scan rate for CO_2 treated samples.

C_{CV} (F/g)	10 mV/s	30 mV/s	50 mV/s
IR1-c12 (tea)	82.9	79.2	76.8
IR1-c36 (tea)	87.1	79.8	75.5
IR1-c900 (tea)	82.1	78.6	76.8
IR4-c12 (tea)	86.2	82.1	79.8
IR4-c36 (tea)	83.3	80.8	79.5
IR4-c900 (tea)	84	80.4	78.6
IR1-c12 (tba)	53.8	48.6	45.7
IR1-c36 (tba)	52.6	45.6	43.3
IR1-c900 (tba)	56.8	52.9	50.9
IR4-c12 (tba)	64.7	62.6	61.4
IR4-c36 (tba)	62.9	59.6	57.9
IR4-c900 (tba)	62.6	59.3	57.4

capacitance reduction of narrow pore size 1 impregnation ratio samples in $TBAPF_6$ electrolyte results from their porous characteristics. As a result, as high as 87 F/g specific capacitance was achieved in sample IR1-c36 at 10 mV/s scan rate.

Conclusions

Activated carbons with various structural and textural characteristics were produced with a combined chemical and physical route. $ZnCl_2$ and CO_2 were used as chemical and physical activating agents, respectively. Their porous textures are affected mainly by impregnation ratio and burn off degree. Only $ZnCl_2$ activated samples at 500 °C have large number of surface functional groups, identified by FTIR analysis. Their structural evolution is strongly dependent on activation temperature; being more ordered for CO_2 treated samples at elevated temperatures. The fact that samples only activated with $ZnCl_2$ have more surface functional groups and lack ordering dramatically impact electrochemical behavior. As a result of their resistive nature, they did not show ideal capacitive behavior. Therefore, their specific capacitance was only 22 F/g in the best case. Successful electrochemical results were obtained from CO_2 treated samples. Capacitance of CO_2 treated samples was affected by their porosity and electrolyte. The capacitances of EDLC's with smaller size cation electrolyte were superior for all samples. Although specific capacitance do not clearly depend on pore size and surface area, capacitance normalization by available surface area shows that microporous carbons with smaller average pore size is more effective in capacitive storage of ions. As a consequence, 87 F/g specific capacitance was achieved in CO_2 treated activated carbons, nearly 4 times higher than the only $ZnCl_2$ treated ones.

Acknowledgment

During the course of this work, one of us (BP) was supported by TUBITAK with a scholarship under 2214-A International Doctoral Research Fellowship Programme, Grant No. 1059B141501226.

REFERENCES

[1] Su CY, Cheng H, Li W, Liu ZQ, Li N, Hou Z, et al. Atomic modulation of FeCo–nitrogen–carbon bifunctional oxygen electrodes for rechargeable and flexible all-solid-state zinc–air battery. Adv Energy Mater 2017;7:1–12. https://doi.org/10.1002/aenm.201602420.

[2] Li XX, Deng XH, Li QJ, Huang S, Xiao K, Liu ZQ, et al. Hierarchical double-shelled poly(3,4-ethylenedioxythiophene) and MnO_2 decorated Ni nanotube arrays for durable and enhanced energy storage in supercapacitors. Electrochim Acta 2018;264:46–52. https://doi.org/10.1016/j.electacta.2018.01.069.

[3] Cheng H, Li M-L, Su C-Y, Li N, Liu Z-Q. Cu-Co bimetallic oxide quantum dot decorated nitrogen-doped carbon nanotubes: a high-efficiency bifunctional oxygen electrode for Zn-Air batteries. Adv Funct Mater 2017;27. https://doi.org/10.1002/adfm.201701833. 1701833.

[4] Chen GF, Li XX, Zhang LY, Li N, Ma TY, Liu ZQ. A porous perchlorate-doped polypyrrole nanocoating on nickel nanotube arrays for stable wide-potential-window supercapacitors. Adv Mater 2016;28:7680–7. https://doi.org/10.1002/adma.201601781.

[5] Zhang Y, Feng H, Wu X, Wang L, Zhang A, Xia T, et al. Progress of electrochemical capacitor electrode materials: a review. Int J Hydrogen Energy 2009;34:4889–99. https://doi.org/10.1016/j.ijhydene.2009.04.005.

[6] Xu B, Wu F, Mu D, Dai L, Cao G, Zhang H, et al. Activated carbon prepared from PVDC by NaOH activation as electrode materials for high performance EDLCs with non-aqueous electrolyte. Int J Hydrogen Energy 2010;35:632–7. https://doi.org/10.1016/j.ijhydene.2009.10.110.

[7] Kisacikoglu MC, Uzunoglu M, Alam MS. Load sharing using fuzzy logic control in a fuel cell/ultracapacitor hybrid vehicle. Int J Hydrogen Energy 2009;34:1497–507. https://doi.org/10.1016/j.ijhydene.2008.11.035.

[8] Yalcinoz T, Alam M. Improved dynamic performance of hybrid PEM fuel cells and ultracapacitors for portable applications. Int J Hydrogen Energy 2008;33:1932–40. https://doi.org/10.1016/j.ijhydene.2008.01.027.

[9] Wang H, Gao Q, Hu J. High hydrogen storage capacity of porous carbons prepared by using activated carbon. J Am Chem Soc 2009;131:7016–22. https://doi.org/10.1021/ja8083225.

[10] Hynek S, Fuller W, Bentley J. Hydrogen storage by carbon sorption. Int J Hydrogen Energy 1997;22:601–10. https://doi.org/10.1016/S0360-3199(96)00185-1.

[11] Zhou L, Zhou Y, Sun Y. A comparative study of hydrogen adsorption on superactivated carbon versus carbon nanotubes. Int J Hydrogen Energy 2004;29:475–9. https://doi.org/10.1016/S0360-3199(03)00092-2.

[12] Duman G, Onal Y, Okutucu C, Onenc S, Yanik J. Production of activated carbon from pine cone and evaluation of its

physical, chemical, and adsorption properties. Energy Fuels 2009;23:2197–204. https://doi.org/10.1021/ef800510m.
[13] Haykiri-Açma H. Combustion characteristics of different biomass materials. Energy Convers Manag 2003;44:155–62. https://doi.org/10.1016/S0196-8904(01)00200-X.
[14] Zhang R, Duan XJ, Guo QG, Zhou B, Liu XM, Jin ML, et al. Effects of ash contents of activated carbon on the performance of electric double layer capacitors. Adv Mater Res 2011;287–290:1469–76. 10.4028, www.scientific.net/AMR.287-290.1469.
[15] Karthikeyan K, Amaresh S, Lee SN, Sun X, Aravindan V, Lee Y-G, et al. Construction of high-energy-density supercapacitors from pine-cone-derived high-surface-area carbons. ChemSusChem 2014;7:1435–42. https://doi.org/10.1002/cssc.201301262.
[16] Bello A, Manyala N, Barzegar F, Khaleed AA, Momodu DY, Dangbegnon JK. Renewable pine cone biomass derived carbon materials for supercapacitor application. RSC Adv 2016;6:1800–9. https://doi.org/10.1039/C5RA21708C.
[17] Genovese M, Lian K. Polyoxometalate modified pine cone biochar carbon for supercapacitor electrodes. J Mater Chem A 2017;5:3939–47. https://doi.org/10.1039/C6TA10382K.
[18] Barbieri O, Hahn M, Herzog A, Kötz R. Capacitance limits of high surface area activated carbons for double layer capacitors. Carbon N Y 2005;43:1303–10. https://doi.org/10.1016/j.carbon.2005.01.001.
[19] Ma Y. Comparison of activated carbons prepared from wheat straw via $ZnCl_2$ and KOH activation. Waste Biomass Valorization 2017;8:549–59. https://doi.org/10.1007/s12649-016-9640-z.
[20] Ma G, Guo D, Sun K, Peng H, Yang Q, Zhou X, et al. Cotton-based porous activated carbon with a large specific surface area as an electrode material for high-performance supercapacitors. RSC Adv 2015;5:64704–10. https://doi.org/10.1039/C5RA11179J.
[21] Ma G, Li J, Sun K, Peng H, Feng E, Lei Z. Tea-leaves based nitrogen-doped porous carbons for high-performance supercapacitors electrode. J Solid State Electrochem 2017;21:525–35. https://doi.org/10.1007/s10008-016-3389-y.
[22] He X, Ling P, Yu M, Wang X, Zhang X, Zheng M. Rice husk-derived porous carbons with high capacitance by $ZnCl_2$ activation for supercapacitors. Electrochim Acta 2013;105:635–41. https://doi.org/10.1016/j.electacta.2013.05.050.
[23] Rufford TE, Hulicova-Jurcakova D, Fiset E, Zhu Z, Lu GQ. Double-layer capacitance of waste coffee ground activated carbons in an organic electrolyte. Electrochem Commun 2009;11:974–7. https://doi.org/10.1016/j.elecom.2009.02.038.
[24] He X, Ling P, Qiu J, Yu M, Zhang X, Yu C, et al. Efficient preparation of biomass-based mesoporous carbons for supercapacitors with both high energy density and high power density. J Power Sources 2013;240:109–13. https://doi.org/10.1016/j.jpowsour.2013.03.174.
[25] Rodríguez-Reinoso F, Molina-Sabio M. Activated carbons from lignocellulosic materials by chemical and/or physical activation: an overview. Carbon N Y 1992;30:1111–8. https://doi.org/10.1016/0008-6223(92)90143-K.
[26] Caturla F, Molina-Sabio M, Rodríguez-Reinoso F. Preparation of activated carbon by chemical activation with $ZnCl_2$. Carbon N Y 1991;29:999–1007. https://doi.org/10.1016/0008-6223(91)90179-M.
[27] Ahmadpour A, Do DD. The preparation of active carbons from coal by chemical and physical activation. Carbon N Y 1996;34:471–9.
[28] Kaneko K, Ishii C, Ruike M, Kuwabara H. Origin of superhigh surface area and microcrystalline graphitic structures of activated carbons. Carbon N Y 1992;30:1075–88. https://doi.org/10.1016/0008-6223(92)90139-N.
[29] Centeno TA, Stoeckli F. The assessment of surface areas in porous carbons by two model-independent techniques, the DR equation and DFT. Carbon N Y 2010;48:2478–86. https://doi.org/10.1016/j.carbon.2010.03.020.
[30] Brunauer S, Deming LS, Deming WE, Teller E. On a Theory of the van der Waals Adsorption of Gases. J Am Chem Soc 1940;62:1723–32. https://doi.org/10.1021/ja01864a025.
[31] Khalili NR, Campbell M, Sandi G, Golaś J. Production of micro- and mesoporous activated carbon from paper mill sludge. I. Effect of zinc chloride activation. Carbon N Y 2000;38:1905–15. https://doi.org/10.1016/S0008-6223(00)00043-9.
[32] Liou TH. Development of mesoporous structure and high adsorption capacity of biomass-based activated carbon by phosphoric acid and zinc chloride activation. Chem Eng J 2010;158:129–42. https://doi.org/10.1016/j.cej.2009.12.016.
[33] Shen W, Li Z, Liu Y. Surface chemical functional groups modification of porous carbon. Recent Pat Chem Eng 2010;1:27–40. https://doi.org/10.2174/1874478810801010027.
[34] Lua AC, Yang T. Characteristics of activated carbon prepared from pistachio-nut shell by zinc chloride activation under nitrogen and vacuum conditions. J Colloid Interface Sci 2005;290:505–13. https://doi.org/10.1016/j.jcis.2005.04.063.
[35] Shin S, Jang J, Yoon S-H, Mochida I. A study on the effect of heat treatment on functional groups of pitch based activated carbon fiber using FTIR. Carbon N Y 1997;35:1739–43. https://doi.org/10.1016/S0008-6223(97)00132-2.
[36] Figueiredo J, Pereira MF, Freitas MM, Órfão JJ. Modification of the surface chemistry of activated carbons. Carbon N Y 1999;37:1379–89. https://doi.org/10.1016/S0008-6223(98)00333-9.
[37] Dandekar A, Baker RTK, Vannice MA. Characterization of activated carbon, graphitized carbon fibers and synthetic diamond powder using TPD and DRIFTS. Carbon N Y 1998;36:1821–31. https://doi.org/10.1016/S0008-6223(98)00154-7.
[38] Seredych M, Hulicova-Jurcakova D, Lu GQ, Bandosz TJ. Surface functional groups of carbons and the effects of their chemical character, density and accessibility to ions on electrochemical performance. Carbon N Y 2008;46:1475–88. https://doi.org/10.1016/j.carbon.2008.06.027.
[39] Lazzarini A, Piovano A, Pellegrini R, Leofanti G, Agostini G, Rudić S, et al. A comprehensive approach to investigate the structural and surface properties of activated carbons and related Pd-based catalysts. Catal Sci Technol 2016;6:4910–22. https://doi.org/10.1039/C6CY00159A.
[40] Blankenship TS, Balahmar N, Mokaya R. Oxygen-rich microporous carbons with exceptional hydrogen storage capacity. Nat Commun 2017;8. https://doi.org/10.1038/s41467-017-01633-x.
[41] Tuinstra F, Koenig JL. Raman spectrum of graphite. J Chem Phys 1970;53:1126–30. https://doi.org/10.1063/1.1674108.
[42] Ferrari AC, Robertson J. Interpretation of Raman spectra of disordered and amorphous carbon. Phys Rev B 2000;61:14095–107. https://doi.org/10.1103/PhysRevB.61.14095.
[43] Dillon RO, Woollam JA, Katkanant V. Use of Raman scattering to investigate disorder and crystallite formation in as-deposited and annealed carbon films. Phys Rev B 1984;29:3482–9. https://doi.org/10.1103/PhysRevB.29.3482.
[44] Fung AWP, Rao AM, Kuriyama K, Dresselhaus MS, Dresselhaus G, Endo M, et al. Raman scattering and electrical conductivity in highly disordered activated carbon fibers. J Mater Res 1993;8:489–500. https://doi.org/10.1557/JMR.1993.0489.

Please cite this article in press as: Köse KÖ, et al., Chemical and structural optimization of $ZnCl_2$ activated carbons via high temperature CO_2 treatment for EDLC applications, International Journal of Hydrogen Energy (2018), https://doi.org/10.1016/j.ijhydene.2018.03.222

[45] Mrozowski S. Electronic properties and band model of carbons. Carbon N Y 1971;9:97–109. https://doi.org/10.1016/0008-6223(71)90123-0.
[46] Pandolfo AG, Hollenkamp AF. Carbon properties and their role in supercapacitors. J Power Sources 2006;157:11–27. https://doi.org/10.1016/j.jpowsour.2006.02.065.
[47] Zhao J, Dai Y, Xu J, Chen S, Xie J. Synthesis and electrochemical characterization of mesoporous carbons prepared by chemical activation. J Electrochem Soc 2008;155:A475. https://doi.org/10.1149/1.2907747.
[48] Chmiola J, Yushin G, Gogotsi Y, Portet C, Simon P, Taberna PL. Anomalous increase in carbon capacitance at pore sizes less than 1 nanometer. Science 2006;313:1760–3. https://doi.org/10.1126/science.1132195.
[49] Chmiola J, Largeot C, Taberna PL, Simon P, Gogotsi Y. Desolvation of ions in subnanometer pores and its effect on capacitance and double-layer theory. Angew Chem Int Ed 2008;47:3392–5. https://doi.org/10.1002/anie.200704894.
[50] Mysyk R, Raymundo-Piñero E, Pernak J, Béguin F. Confinement of symmetric tetraalkylammonium ions in nanoporous carbon electrodes of electric double-layer capacitors. J Phys Chem C 2009;113:13443–9. https://doi.org/10.1021/jp901539h.
[51] Mysyk R, Raymundo-Piñero E, Béguin F. Saturation of subnanometer pores in an electric double-layer capacitor. Electrochem Commun 2009;11:554–6. https://doi.org/10.1016/j.elecom.2008.12.035.
[52] Shi H. Activated carbons and double layer capacitance. Electrochim Acta 1996;41:1633–9. https://doi.org/10.1016/0013-4686(95)00416-5.
[53] Ania CO, Pernak J, Stefaniak F, Raymundo-Piñero E, Béguin F. Polarization-induced distortion of ions in the pores of carbon electrodes for electrochemical capacitors. Carbon N Y 2009;47:3158–66. https://doi.org/10.1016/j.carbon.2009.06.054.

Please cite this article in press as: Köse KÖ, et al., Chemical and structural optimization of $ZnCl_2$ activated carbons via high temperature CO_2 treatment for EDLC applications, International Journal of Hydrogen Energy (2018), https://doi.org/10.1016/j.ijhydene.2018.03.222